Obrabotka metallov (tekhnologiya, oborudovanie, instrumenty) = Metal Working and Material Science. 2026 vol. 28 no. 3 pp. 83–111
ISSN: 1994-6309 (print) / 2541-819X (online)
DOI: 10.17212/1994-6309-2026-28.3-83-111

NSTU NETI

Obrabotka metallov - Metal Working and Material Science

Journal homepage: http://journals.nstu.ru/obrabotka_metallov

Influence of high-frequency electromagnetic field-assisted TIG surface modification on microstructural evolution, elemental redistribution and hardness of EN-GJV-400 compacted graphite iron

Farhad Mahammad oglu Shirzadov [a, *]

Azerbaijan Technical University, 25 H. Javid Avenue, Baku, AZ1073, Azerbaijan

[a] https://orcid.org/0009-0006-9378-9865, farhad.shirzadov@aztu.edu.az

ARTICLE INFO

Article history:
Received: 07 July 2026
Revised: 15 July 2026
Accepted: 17 July 2026
Available online: 15 September 2026

Keywords:
EN-GJV-400
TIG remelting
High-frequency electromagnetic field
Solidification behavior
Surface engineering

Acknowledgments
The author acknowledges that part of the experimental investigations was conducted at the Technical University of Berlin (Germany) within the framework of scientific cooperation and research activities related to surface engineering technologies. The authors' current institutional affiliation is Azerbaijan Technical University, where the research work was further developed and prepared for publication. The experimental facilities and scientific support provided during the research stay at TU Berlin are gratefully acknowledged.

ABSTRACT

Introduction. Compacted graphite iron (EN-GJV-400) is widely used for highly loaded automotive and engineering components due to its favourable combination of strength, thermal conductivity, damping capacity and castability. However, the relatively moderate hardness and wear resistance of its surface region may limit its application under severe contact conditions. High-frequency electromagnetic field (HFEMF)-assisted treatment represents a potential approach for modifying solidification conditions and improving structural uniformity during surface engineering. Nevertheless, the influence of HFEMF-assisted TIG treatment on the microstructural evolution, elemental redistribution and hardness response of compacted graphite iron remains insufficiently understood. **Materials and methods.** In this study, conventional and HFEMF-assisted TIG surface modification of EN-GJV-400 compacted graphite iron was investigated. The experimental program included TIG remelting, TIG surface alloying using Ni78Si8B14 and CuSn-4 foils, and TIG hardfacing using UTP A DUR 600 chromium-containing filler wire, performed with and without electromagnetic assistance. A high-frequency electromagnetic field with a frequency of 200 kHz was applied during treatment. The modified surface layers were characterized using optical microscopy, scanning electron microscopy combined with energy-dispersive X-ray spectroscopy (SEM/EDS) and Vickers microhardness measurements. **Results and discussion.** The obtained results indicate that HFEMF-assisted processing influences the structural development of TIG-modified layers by affecting the conditions of heat and mass transfer during melting and solidification. The influence of HFEMF was evaluated indirectly through surface morphology, microstructural characteristics, elemental distribution and hardness response. Conventional TIG remelting increased the surface hardness of EN-GJV-400 from approximately 375 HV0.1 to 765 HV0.1 due to graphite dissolution, carbon redistribution and formation of ledeburitic structures containing cementite-rich constituents. HFEMF-assisted remelting produced a comparable hardness level of approximately 760 HV0.1, indicating that electromagnetic assistance does not act as an independent strengthening mechanism but mainly contributes to structural homogenization. Ni78BSi8B14 alloying resulted in hardened transformation products together with ledeburitic and carbide-containing constituents, while HFEMF primarily improved the uniformity of alloy-element distribution. For UTP A DUR 600 hardfacing, HFEMF-assisted treatment increased the average hardness from approximately 771 HV0.1 to 800 HV0.1, which is attributed to improved redistribution and more uniform formation of chromium-containing hard phases. ***Conclusion.*** The results demonstrate that HFEMF-assisted TIG treatment provides an additional process-control parameter for surface modification of EN-GJV-400 compacted graphite iron. The effectiveness of electromagnetic assistance depends on the chemical composition of the modified layer and the dominant strengthening mechanism. HFEMF should therefore be considered primarily as a method for improving structural uniformity, elemental redistribution and phase distribution rather than as a universal hardness-enhancement technique. Further studies involving direct molten-pool observation and numerical modelling are required to quantitatively establish the relationship between electromagnetic parameters and melt-pool behaviour.

For citation: Shirzadov F.M. Influence of high-frequency electromagnetic field-assisted TİG surface modification on microstructural evolution, elemental redistribution and hardness of EN-GJV-400 compacted graphite iron. *Obrabotka metallov (tekhnologiya, oborudovanie, instrumenty) = Metal Working and Material Science*, 2026, vol. 28, no. 3, pp. 83–111. DOI: 10.17212/1994-6309-2026-28.3-83-111. (In Russian).

*** Corresponding author**
Shirzadov Farhad Mahammad oglu, Ph.D (Engineering),
Associate Professor
Azerbaijan Technical University,
25 H. Javid Avenue,
AZ1073, Baku, Azerbaijan
Tel.: +994559029446, **e-mail:** farhad.shirzadov@aztu.edu.az

Introduction

Surface engineering technologies play a critical role in improving the functional performance and service life of engineering components subjected to severe mechanical, thermal, and tribological loading conditions. Compared with complete component replacement, surface modification methods enable selective enhancement of surface properties while preserving the desirable bulk characteristics of the substrate material. Therefore, processes such as surface remelting, alloying, and cladding are widely applied in automotive, energy, mining, and heavy machinery industries for component restoration, life extension, and performance improvement [1–5].

Compacted graphite iron (*CGI*), particularly the *EN-GJV-400* grade, has attracted considerable attention due to its favorable combination of mechanical strength, thermal conductivity, damping capacity, and castability. The vermicular graphite morphology provides intermediate characteristics between grey and ductile cast irons, enabling its application in highly loaded automotive components such as camshafts, cylinder blocks, and cylinder heads. The specific graphite morphology of *CGI* also makes this material an interesting system for studying the interaction between thermal processing, carbon redistribution, and electromagnetic-assisted modification of molten regions. During *TIG* surface processing, localized melting is accompanied by graphite dissolution, carbon redistribution, and rapid non-equilibrium solidification, resulting in significant microstructural transformation. However, despite its advantageous bulk properties, the service performance of *CGI* components is often restricted by surface degradation mechanisms, including adhesive and abrasive wear, cyclic thermal loading, and contact fatigue, which are associated with the limited hardness and wear resistance of the near-surface region [1–6].

Various surface modification technologies have been developed to enhance the functional properties of cast iron components, including laser remelting, plasma transferred arc (*PTA*) processing, laser cladding, thermal spraying, and tungsten inert gas (*TIG*) surface treatment. These processes involve localized melting followed by rapid solidification, leading to structural transformations such as graphite dissolution, carbon redistribution, formation of ledeburitic eutectic constituents, carbide precipitation and, depending on alloy composition, martensitic transformation. Such microstructural modifications can substantially improve hardness and wear resistance. Although laser-based techniques provide high energy density and precise control of heat input, their industrial implementation may be limited by equipment cost and technological complexity, particularly for large-scale components. In comparison, *TIG* surface modification remains attractive due to its relatively simple equipment requirements, operational flexibility, and suitability for repair and surface treatment of large engineering parts [7–10].

Nevertheless, conventional *TIG* processing provides limited control over molten-pool dynamics during melting and solidification. The evolution of the molten region is governed mainly by arc heat input, Marangoni convection, buoyancy effects, and gravitational forces. The simultaneous action of these phenomena may cause non-uniform material transport, local chemical segregation, variations in solidification conditions, and heterogeneous distribution of structural constituents. Therefore, improving the controllability of transport phenomena during *TIG*-based surface engineering remains an important research challenge, especially for *CGI* materials where graphite dissolution and carbon redistribution strongly influence the final microstructure.

In recent years, the application of external physical fields has emerged as a promising strategy for controlling heat and mass transfer phenomena during welding and surface modification processes. Among these approaches, electromagnetic field-assisted processing has attracted increasing attention due to its capability to influence the behavior of electrically conductive molten metals. When a conductive liquid metal interacts with an external magnetic field, induced electrical currents are generated within the molten region. The interaction between current density and magnetic flux density produces electromagnetic forces described by the *Lorentz* force term, which can modify liquid-phase flow, solute transport, and solidification behavior. The effectiveness of this interaction depends on electromagnetic parameters, material electrical conductivity, magnetic-field distribution, and molten-pool geometry [11–15].

Electromagnetic-assisted technologies have been investigated in casting, welding, additive manufacturing, and surface modification of ferrous and non-ferrous alloys. Previous studies have demonstrated that electromagnetic stirring can improve chemical homogeneity, reduce segregation, modify solidification morphology, and refine structural constituents. However, the final effect of electromagnetic assistance strongly depends on excitation frequency, magnetic-field intensity, interaction volume, material properties, and processing conditions [16–19].

Compared with conventional low-frequency electromagnetic stirring systems, *HFEMF* systems provide localized interaction with electrically conductive molten regions due to their limited electromagnetic penetration depth. This feature is particularly important for surface modification processes, where the treated volume is relatively small and precise control of molten-pool transport phenomena is required. Therefore, *HFEMF* represents a potential approach for modifying near-surface solidification behavior while maintaining the properties of the bulk component.

Despite significant progress in electromagnetic-assisted processing, most previous studies have concentrated on aluminum alloys, steels, casting processes, and welding-based joining technologies. In contrast, the application of *HFEMF* during *TIG* surface modification of compacted graphite iron remains insufficiently investigated. In particular, the relationship between electromagnetic assistance, molten-pool behavior, alloy-element redistribution, microstructural evolution, and hardness response of *CGI* surface layers has not yet been systematically established [20–22].

Furthermore, the influence of *HFEMF* on different *TIG*-based surface modification approaches, including direct remelting, alloying with additional elements, and deposition of carbide-forming cladding materials, requires further clarification. The expected contribution of electromagnetic assistance is likely to depend on the chemical composition of the modified layer and the dominant strengthening mechanisms. In systems where hardness is primarily controlled by rapid solidification of the substrate material, *HFEMF* may mainly contribute to structural homogenization. In alloyed and cladded layers containing carbide-forming elements, electromagnetic-assisted redistribution may influence the formation and spatial arrangement of strengthening phases.

Therefore, ***the objective of this study*** is to investigate the influence of *HFEMF*-assisted *TIG* processing on microstructural evolution, elemental redistribution, and hardness behavior of *EN-GJV-400* compacted graphite iron. Particular attention is given to understanding *HFEMF* as a process-control parameter affecting surface-layer formation, phase distribution, and structural homogeneity under different *TIG* modification conditions.

To achieve this objective, ***the following research tasks*** were addressed:

– to investigate the influence of a 200 kHz *HFEMF* on surface-layer formation and structural uniformity during *TIG* processing of *EN-GJV-400* compacted graphite iron;

– to evaluate the effect of *HFEMF*-assisted processing on microstructural evolution and spatial distribution of structural constituents formed during rapid solidification;

– to analyze the redistribution and homogenization of alloying elements during *HFEMF*-assisted *TIG* alloying with *Ni78Si8B14* and *CuSn-4* foils and *UTP A DUR 600* chromium-containing cladding wire using *SEM*/*EDS* characterization;

– to establish the relationship between *HFEMF*-assisted processing, elemental redistribution, microstructural development, and hardness response of modified surface layers.

Materials and methods

Materials

EN-GJV-400 compacted graphite iron (*CGI*) was selected as the substrate material for *TIG* surface modification and *HFEMF*-assisted processing experiments. *CGI* is widely used for automotive components, including camshafts, due to its combination of mechanical strength, thermal conductivity, damping capacity, and castability. However, the relatively limited hardness and wear resistance of the near-surface region restrict its performance under severe contact loading conditions.

The investigated specimens were manufactured from commercial *EN-GJV-400* camshafts, and the specimen geometry is shown in Fig. 1.

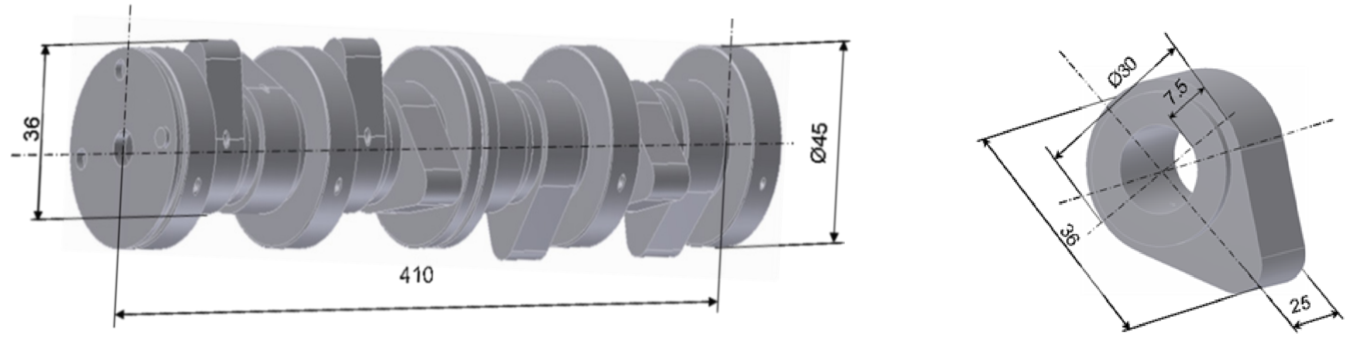

Fig. 1. Geometry of the EN-GJV-400 compacted graphite iron camshaft specime

The initial microstructure of *EN-GJV-400* consists of a ferritic-pearlitic matrix containing uniformly distributed vermicular graphite particles. The chemical composition of the substrate material is presented in Table 1.

Table 1

Chemical composition of *EN-GJV-400* compacted graphite iron used as the substrate material

Substrate material	*C*	*Si*	*Al*	*Mn*	*Cr*	*Cu*	*Ni*
EN-GJV-400	2.7–3.8	0.5–2.9	<0.1	0.2–0.6	<0.1	0.6–1.0	0.2–0.6

A chromium-containing cladding wire, *UTP A DUR 600*, was selected for *TIG* cladding experiments. The filler material contains approximately 9.5 wt.% chromium and was chosen due to its carbide-forming capability during rapid solidification. The formation and distribution of chromium-rich carbide-containing hard phases provide increased hardness and improved wear resistance of the deposited surface layer. The nominal chemical composition and hardness of the filler wire are summarized in Table 2.

Table 2

Chemical composition and nominal hardness of *UTP A DUR 600* filler wire used for *TIG* cladding

Filler wire	*C*	*Si*	*Mn*	*Cr*	Balance	Nominal hardness
UTP A DUR 600	0.5	3.0	0.5	9.5	Fe	610 HV

To investigate the influence of controlled alloying on the formation and functional properties of modified *EN-GJV-400* surfaces, two alloying foils, *Ni78Si8B14* and *CuSn-4*, were employed.

The *Ni78Si8B14* alloy was selected because *Ni*, *Si,* and *B* are known to increase hardenability and promote the formation of hard phases during rapid solidification. The introduction of these elements increases the hardenability of the molten zone and promotes the formation of martensitic constituents together with ledeburitic and carbide-containing phases during rapid cooling. In addition, nickel alloying was investigated due to its ability to modify the interaction between the molten metal and graphite phase, allowing preservation of graphite-containing regions that are beneficial for tribological performance because graphite acts as a solid lubricant during sliding contact.

The *CuSn-4* foil was used to introduce copper-rich regions into the modified surface layer. Unlike chromium-based cladding, the objective of copper alloying was not maximum hardness enhancement but modification of tribological behavior. Copper-containing regions are generally reported to facilitate the formation of transfer films during sliding contact and may reduce direct metal-to-metal interaction. In the present work, this potential tribological benefit is discussed only as a hypothesis based on the expected role of *Cu*-rich regions, since no tribological experiments were performed.

The chemical compositions and intended functional roles of the alloying foils are presented in Table 3.

Table 3

Chemical composition and functional role of *Ni78Si8B14* and *CuSn-4* alloying foils used for TIG surface alloying of *EN-GJV-400*

Alloying foil	*Ni* (wt.%)	*Si* (wt.%)	*B* (wt.%)	*Cu* (wt.%)	*Sn* (wt.%)	Proposed functional role
Ni78Si8B14	78	8	14	–	–	Modification of phase formation processes, increased hardenability, formation of martensitic and carbide-containing structural constituents, retention of graphite phase benefits for tribological properties
CuSn-4	–	–	–	95–97	3–5	Formation of copper-containing regions, modification of surface friction behavior, possible formation of transfer films during wear

Experimental procedure

Surface modification experiments were carried out using a *TIG 200* AC/DC welding power source coupled with a *TTH15* induction heating system (15 kW) capable of generating an *HFEMF* of up to 450 kHz. A water-cooled coil-type copper inductor was used to generate the alternating electromagnetic field around the *TIG* processing zone. The inductor consisted of a multi-turn copper coil positioned concentrically around the processing region, providing electromagnetic coupling between the applied magnetic field and the electrically conductive molten pool. The distance between the inductor and the molten zone was adjusted to achieve effective *Lorentz*-force interaction while maintaining stable *TIG* arc operation.

In the present study, a constant electromagnetic field frequency of 200 kHz was applied during *HFEMF*-assisted processing. Since direct magnetic flux density measurement during *TIG* operation was not available, induction power was used as the controlled electromagnetic parameter. The induction power was varied within the range of 25–100% depending on the investigated surface modification process to control the intensity of electromagnetic stirring while maintaining stable arc operation.

The experimental program included three types of surface treatments:

– *TIG* remelting of *EN-GJV-400* compacted graphite iron,

– *TIG* surface cladding using *UTP A DUR 600* cladding wire,

– *TIG* surface alloying using *CuSn-4* and *Ni78Si8B14* foils.

Conventional *TIG* remelting without electromagnetic assistance was used as the reference condition.

For all *HFEMF*-assisted experiments, the welding current was adjusted according to the applied treatment mode, while the electromagnetic system parameters were maintained constant to ensure comparable processing conditions. A frequency of 200 kHz was selected based on preliminary experiments, which demonstrated stable arc operation and reliable electromagnetic coupling between the applied field and the electrically conductive molten pool.

A non-consumable tungsten electrode with a diameter of 2.4 mm was used. High-purity argon was supplied as shielding gas during all processing operations to prevent oxidation and atmospheric contamination of the molten zone.

The schematic configuration of the *TIG–HFEMF* experimental setup is shown in Fig. 2. The processing parameters used for surface cladding, remelting, and alloying experiments are summarized in Tables 4–6.

For comparative analysis, the *TIG* processing parameters were maintained identical for conventional and *HFEMF*-assisted conditions.

Cam surface alloying under an *HFEMF* was performed according to the configuration shown in Fig. 3, where the coupling between *TIG* arc heating and electromagnetic induction generates *Lorentz*-force-driven melt-pool flow. This interaction governs the redistribution of alloying elements and stabilizes the solidification front, enabling controlled formation of the modified surface layer.

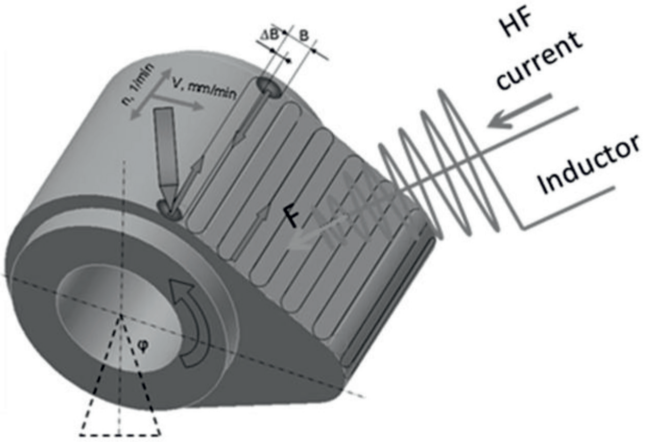

Geometrical Parameters
- Melt pool dimensions
- Weld bead overlap
- Electrode angle and stand-off distance
- Surface layer geometry

Processing Parameters
- Welding speed
- Welding current
- Arc voltage
- Electromagnetic field frequency
- Electromagnetic field intensity

Fig. 2. Schematic configuration of the *TIG-HFEMF* experimental system for surface modification of *EN-GJV-400* compacted graphite iron

Table 4

Treatment parameters used for *TIG* cladding with *UTP A DUR 600* filler wire under *HFEMF*-assisted conditions

Parameter	Value
Welding current	30–130 A
Bead height	<3 mm
Travel speed	50–130 mm/min
Electrode oscillation frequency	20–40 min^{-1}
Electrode stick-out	2.0–2.5 mm
Bead width	5–6 mm
Filler wire diameter	3.2 mm
Induction power	25–100%
Electromagnetic field frequency	200 kHz
Argon flow rate	8 L/min

Table 5

Process conditions used for *TIG* remelting of *EN-GJV-400* compacted graphite iron under *HFEMF*-assisted condition

Parameter	Value
Welding current	40–140 A
Penetration depth	<2.5 mm
Travel speed	90–150 mm/min
Electrode oscillation frequency	40–90 min^{-1}
Electrode stick-out	2.0–2.5 mm
Melted zone width	4–6 mm
Induction power	25–100%
Electromagnetic field frequency	200 kHz
Argon flow rate	8 L/min

Table 6

Process conditions used for *TIG* surface alloying of *EN-GJV-400* compacted graphite iron under *HFEMF*-assisted conditions

Parameter	Value
Welding current	80–145 A
Penetration depth	<3.5 mm
Travel speed	40–70 mm/min
Electrode oscillation frequency	20–70 min^{-1}
Electrode stick-out	2.0–3.5 mm
Melted zone width	5–7 mm
Induction power	25–100%
Electromagnetic field frequency	200 kHz
Argon flow rate	6 L/min

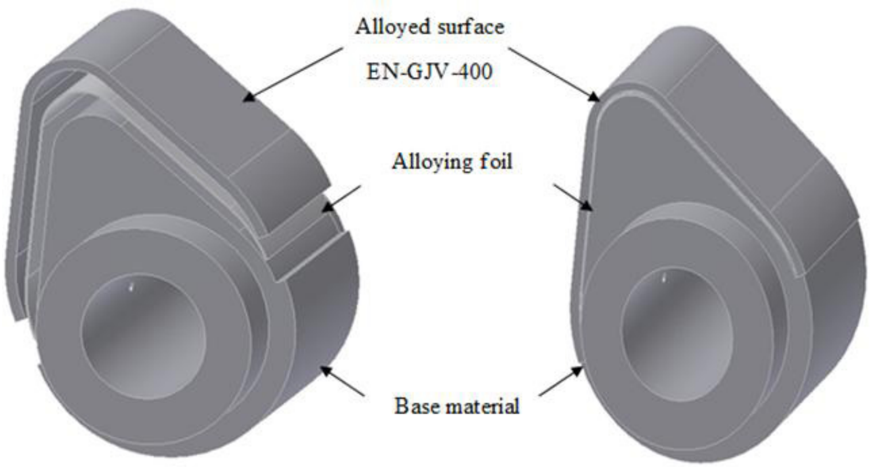

Fig. 3. Schematic illustration of *HFEMF*-assisted *TIG* surface alloying of *EN-GJV-400* using *Ni78Si8B14* and *CuSn-4* alloying foils

The required amount of alloying material introduced into the molten zone was calculated before processing to ensure controlled chemical modification of the surface layer. The calculation was based on the thickness of the treated surface area ($\boldsymbol{h_R}$), foil thickness ($\boldsymbol{h_f}$), and alloy concentration in the alloying foil ($\boldsymbol{E_L}$).

$$h_R(\text{mm}) + h_F(\text{mm}) \to 100\,\%;$$

$$E_V = \frac{h_F}{h_R + h_F} \cdot 100\,\% \cdot \left(\frac{E_L\,\%}{100\,\%}\right);$$

$$h_f(m) \to E_V\,\%; \qquad (1)$$

$$E_V = \frac{E_L h_F}{h_R - h_F},$$

where $\boldsymbol{E_V}$ is the required amount of alloying elements on the surface to be treated; $\boldsymbol{h_R}$ is the thickness of the deposited (coated) layer; $\boldsymbol{h_f}$ is the thickness of the alloying foil; $\boldsymbol{E_L}$ is the concentration (mass fraction) of the alloying element in the foil.

Once the required amount of alloying element in the molten zone is defined, the necessary foil thickness is determined using the following inverse relationship, enabling precise control of chemical input and ensuring consistent alloying conditions within the melt pool during *TIG* surface cladding.

$$h_F = \frac{h_R E_V}{E_L - E_V}. \quad (2)$$

Surface preparation and microstructural characterization

After *TIG* remelting, surface alloying, and cladding treatments, the specimens were sectioned perpendicular to the modified tracks to investigate the evolution of the surface layer structure and chemical composition. The cross-sectional surfaces were prepared by conventional metallographic procedures, including grinding and polishing. The final surface preparation step was performed using fine polishing media to achieve a surface roughness below 3 μm, which ensured reliable optical and electron microscopy observations.

The prepared specimens were chemically etched using an appropriate metallographic etchant for cast iron and alloyed surface layers to reveal the characteristic microstructural constituents, including graphite morphology, matrix phases, carbide-containing regions, and solidification-related features within the modified layers.

Optical microstructural investigations were performed using a *Leica* optical microscope. *The* analysis was carried out on the cross-sections of the untreated substrate, *TIG*-remelted zones, electromagnetic-field-assisted remelted layers, alloyed regions, and cladded coatings. Particular attention was given to the morphology of the remelted zone, the transition region between the modified layer and the substrate, and the distribution of newly formed structural constituents.

The phase and elemental evolution within the modified surface layers were investigated using scanning electron microscopy (*SEM*) combined with energy-dispersive X-ray spectroscopy (*EDS*). Elemental analyses were performed using a *CAMEBAX MICROBEAM* electron microprobe system manufactured by *CAMECA*, equipped with a silicon semiconductor detector and an analog-digital signal processing system. The *EDS* measurements were carried out within selected regions of the modified layers to evaluate the redistribution and homogenization of alloying elements induced by *HFEMF*-assisted melt-pool stirring.

It should be noted that *EDS* analysis provides semi-quantitative information for medium- and high-atomic-number elements. Because of the low characteristic X-ray energy of boron and the limited sensitivity of *EDS* for light elements, the boron content introduced by the *Ni78Si8B14* alloy was not quantified directly. Similarly, the measured carbon concentration was not used for quantitative interpretation due to possible errors associated with graphite morphology, interaction volume, and surface preparation. Therefore, the *EDS* results presented in this work were used primarily to evaluate the redistribution of *Ni*, *Cu*, and *Cr*, whereas the role of boron and carbon in phase formation was interpreted based on the nominal alloy composition together with the observed microstructural evolution and hardness response.

During *EDS* analysis, characteristic X-ray signals generated by electron-beam interaction with the specimen were collected and processed for elemental identification and quantitative analysis. Measurements were performed on representative areas of the alloyed and cladded layers, including the surface region, middle part of the modified layer, and the interface zone with the *EN-GJV-400* substrate. This approach enabled evaluation of the effect of *Lorentz*-force-driven melt convection on the distribution of alloying elements.

Microhardness measurements were performed using a *PMT-3* microhardness tester. The applied load and measurement conditions were kept constant for all specimens to ensure comparability of the obtained results.

The combined use of optical microscopy, *SEM*/*EDS* elemental analysis, and microhardness measurements provided an evaluation of the relationship between electromagnetic-field-assisted processing conditions, chemical redistribution, microstructural evolution, and mechanical response of the modified *EN-GJV-400* surfaces.

Experimental matrix

To systematically evaluate the influence of *HFEMF*-assisted *TIG* processing on the surface modification behavior of *EN-GJV-400* compacted graphite iron, an experimental matrix was developed considering both conventional *TIG* processing and *HFEMF*-assisted conditions.

The investigated surface modification routes included:

– conventional *TIG* remelting,

– *HFEMF*-assisted *TIG* remelting,

– *TIG* surface alloying with *Ni78Si8B14* and *CuSn-4* foils with and without electromagnetic assistance,

– *TIG* claddung using *UTP A DUR 600* chromium-rich filler wire with and without *HFEMF*.

The applied electromagnetic field frequency was maintained at 200 kHz for all *HFEMF*-assisted experiments. The induction power was adjusted according to the processing condition to ensure stable electromagnetic stirring without disturbing arc stability. Conventional *TIG* treatments without electromagnetic assistance were used as reference conditions for evaluating the specific contribution of *HFEMF*.

The experimental design was established to distinguish between:

– the influence of electromagnetic stirring on melt-pool behavior and structural homogenization;

– the effect of alloying elements on phase formation and hardness development;

– the interaction between *HFEMF* and carbide-forming alloy systems.

The untreated *EN-GJV-400* substrate was designated as the reference material. *TIG* remelting conditions were used to evaluate the effect of rapid thermal cycling and self-quenching on graphite dissolution, carbon redistribution, and formation of hardened ledeburitic structures. *Ni78Si8B14* alloying was selected to investigate the formation of martensitic and carbide-containing phases due to increased hardenability, whereas *CuSn-4* alloying was applied to modify surface behavior while maintaining graphite-related functional properties. *UTP A DUR 600* cladding was selected to evaluate the influence of *HFEMF* on chromium-rich carbide formation and cladding performance.

The complete experimental matrix is summarized in Table 7.

Table 7

Experimental matrix of the investigated *EN-GJV-400* surface modification conditions and the objectives of each treatment

Sample	Surface treatment type	*HFEMF*	Frequency	Main research objective
S0	Cast iron *EN-GJV-400*	No	–	Initial microstructure and initial microhardness
S1	Conventional *TIG* remelting	No	–	Investigation of graphite dissolution, carbon redistribution and formation of ledeburitic structure
S2	*TIG* remelting + *HFEMF*	Yes	200 kHz	Evaluation of *HFEMF* effect on structural homogeneity and solidification characteristics
S3	*TIG* alloying with *Ni78Si8B14*	No	–	Investigation of *Ni–Si–B* alloying effect on phase formation and formation of martensitic and carbide-containing structures
S4	*TIG* alloying with *Ni78Si8B14 + HFEMF*	Yes	200 kHz	Investigation of *HFEMF* effect on alloying element redistribution and phase composition homogeneity
S5	*TIG* alloying with *CuSn-4*	No	–	Investigation of copper alloying effect and retention of graphite phase functional properties
S6	TIG alloying with *CuSn-4+HFEMF*	Yes	200 kHz	Investigation of copper redistribution and structural homogeneity under electromagnetic stirring
S7	*TIG* cladding with *UTP A DUR 600*	No	–	Investigation of chromium-containing cladding structure and carbide phase formation
S8	*TIG* cladding with *UTP A DUR 600 + HFEMF*	Yes	200 kHz	Determination of *HFEMF* effect on chromium carbide distribution and hardness enhancement

Results and discussion

Surface morphology

The surface morphology of the *EN-GJV-400* camshaft specimens after *TIG* surface treatment was evaluated to determine the influence of *HFEMF* assistance on melt-pool stability and surface layer formation. A comparison was performed between conventional *TIG* remelting and *HFEMF*-assisted *TIG* processing. The corresponding surface appearances after polishing are presented in Figs. 4 and 5.

Fig. 4 shows the surface condition obtained after conventional *TIG* remelting. Although a continuous remelted track was formed, noticeable geometric irregularities and local deviations along the cam profile were observed. These features indicate non-uniform molten metal redistribution during processing. Under conventional *TIG* conditions, melt-pool behavior is governed mainly by arc heat distribution, surface tension gradients, and gravitational effects. The absence of external melt-flow control results in asymmetric material transport, particularly during horizontal processing of the cam geometry, where gravity promotes preferential molten metal displacement toward lower regions of the pool.

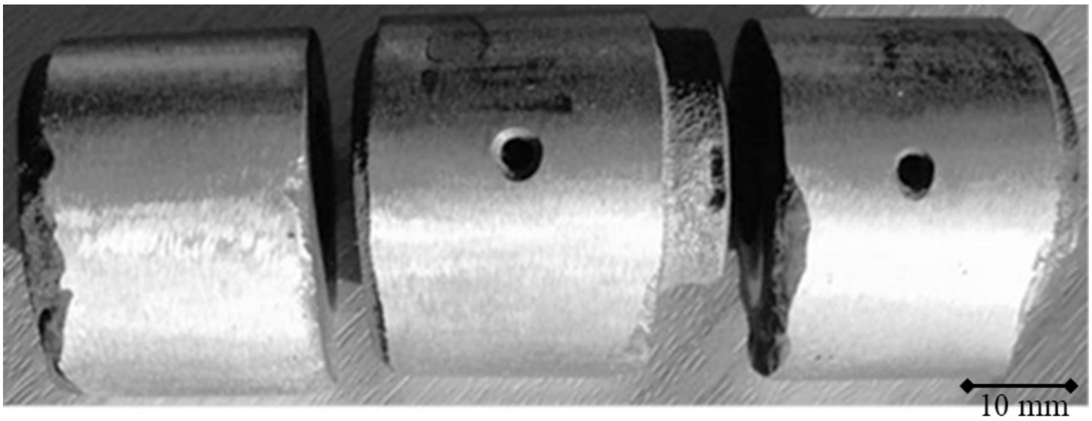

Fig. 4. Surface morphology of *EN-GJV-400* camshaft after conventional *TIG* remelting

Such uncontrolled melt redistribution leads to variations in the remelted layer geometry, including local accumulation of molten material and deviations from the original surface profile. These effects may negatively influence the dimensional accuracy of repaired cam surfaces and subsequently affect contact conditions during operation.

In contrast, the specimens processed under *HFEMF*-assisted *TIG* remelting exhibited a more uniform surface morphology, as shown in Fig. 5. The application of the electromagnetic field resulted in a more uniform surface morphology, which may be associated with modified heat and mass transfer conditions during processing. Compared with conventional *TIG* processing, the *HFEMF*-assisted specimens demonstrated smoother surface contours, reduced edge deformation, and improved conformity with the original cam geometry.

The improved surface uniformity can be attributed to the interaction between the induced electrical currents and the applied magnetic field, which generated electromagnetic forces within the conductive molten pool. These electromagnetic interactions are considered to influence liquid-phase transport phenomena during processing. As a result, more balanced heat and mass transfer conditions were achieved, contributing to improved melt-pool stability and more controlled solidification.

The effect of electromagnetic assistance became more pronounced with increasing induction power, as higher electromagnetic excitation was associated with improved surface uniformity, which may indicate modified melt transport conditions during processing. This behavior confirms that *HFEMF* provides an additional approach for influencing molten-region transport conditions and improving surface layer uniformity during *TIG* surface modification.

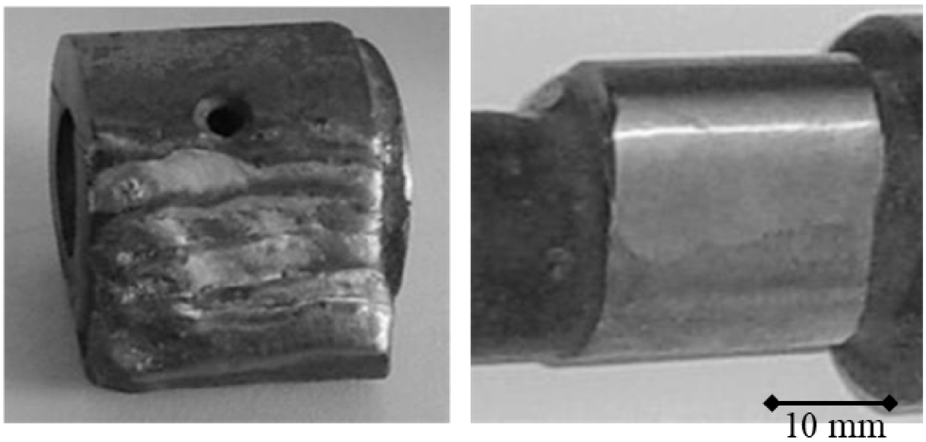

Fig. 5. Surface morphology of *EN-GJV-400* camshaft after *HFEMF*-assisted *TIG* remelting

Microstructural evolution

The microstructural evolution of *EN-GJV-400 CGI* after *TIG* remelting, surface alloying, and cladding was investigated to clarify the role of *HFEMF* assistance in phase formation, elemental redistribution, and structural homogenization. The analysis was performed using optical microscopy and scanning electron microscopy on cross-sectional specimens prepared from the modified surface layers.

Fig. 6 presents the initial microstructure of the as-received *EN-GJV-400* compacted graphite iron. The substrate consists of a ferritic-pearlitic matrix containing uniformly distributed vermicular graphite particles, which is characteristic of compacted graphite iron used for automotive applications.

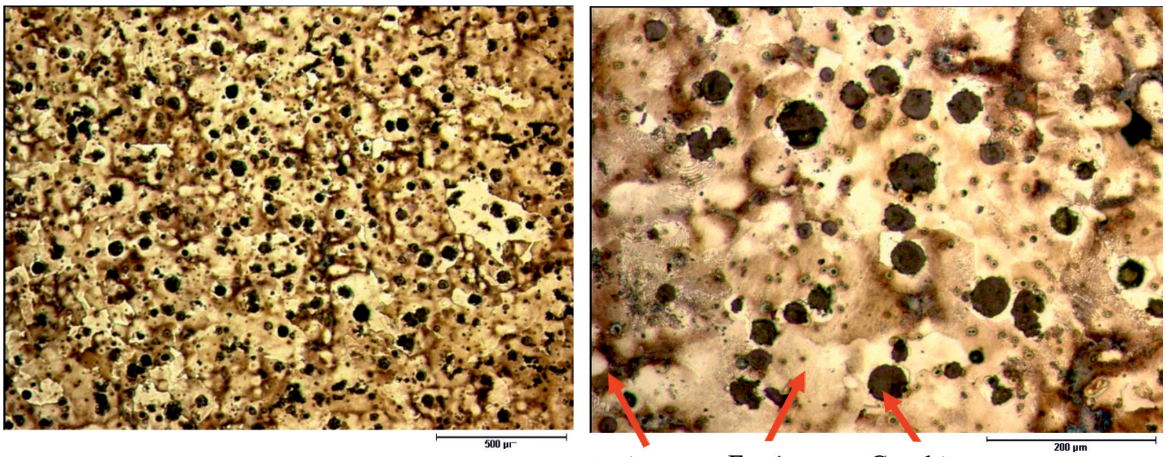

a *b*

Fig. 6. Initial microstructure of the as-received *EN-GJV-400 CGI* substrate. Etched with 2% nital; magnification ×100 (*a*) and ×200 (*b*); scale bars: 500 μm and 200 μm

The presence and morphology of graphite strongly influence the subsequent transformation behaviour during *TIG* processing. During rapid heating, part of the graphite dissolves into the molten iron matrix, increasing the local carbon concentration in the melt pool. Subsequent rapid cooling under non-equilibrium conditions promotes the formation of hard transformation products and eutectic constituents within the modified surface layer.

Fig. 7 compares the microstructures obtained after conventional *TIG* remelting and *HFEMF*-assisted *TIG* remelting of *EN-GJV-400*.

After conventional *TIG* remelting, the initial ferritic-pearlitic structure is transformed into a hardened surface layer consisting mainly of ledeburitic eutectic constituents with cementite-rich phases formed

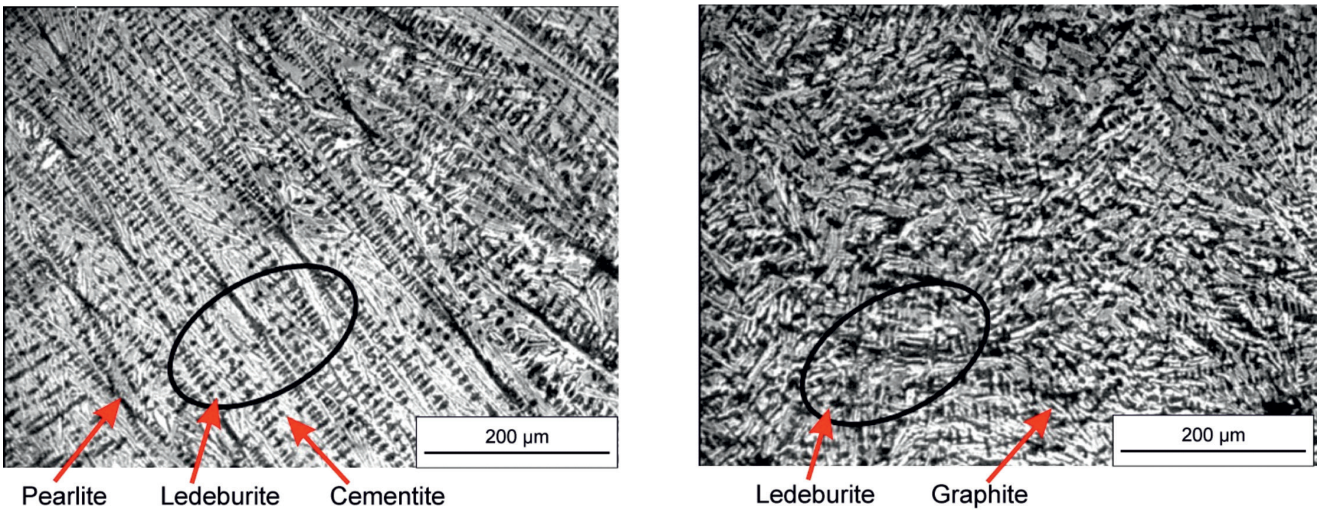

a *b*

Fig. 7. Microstructural comparison of *EN-GJV-400* surface layers after conventional *TIG* remelting (*a*) and *HFEMF*-assisted *TIG* remelting (*b*). Etched with 3% nital; magnification ×200; scale bar: 200 µm

during rapid solidification. The formation of these hard structural components is associated with dissolution of graphite particles, carbon enrichment of the molten zone, and subsequent non-equilibrium solidification.

The conventionally remelted layer exhibits a heterogeneous morphology due to non-uniform heat transfer and limited melt-pool circulation. Local variations in carbon distribution and solidification rate result in spatial differences in the morphology and distribution of eutectic constituents.

Under *HFEMF*-assisted *TIG* remelting, the same general solidification mechanism is maintained; however, the morphology and spatial distribution of structural constituents become more uniform. The electromagnetic field is considered to induce Lorentz-force-assisted convection within the electrically conductive molten region.

Therefore, *HFEMF* does not fundamentally change the phase formation mechanism during *TIG* remelting of *EN-GJV-400*. Its primary effect is associated with improved homogenization of the ledeburitic structure and more uniform distribution of carbon-rich regions within the modified layer.

Fig. 8 shows the microstructures of *UTP A DUR 600* cladded layers produced under conventional *TIG* and *HFEMF*-assisted conditions.

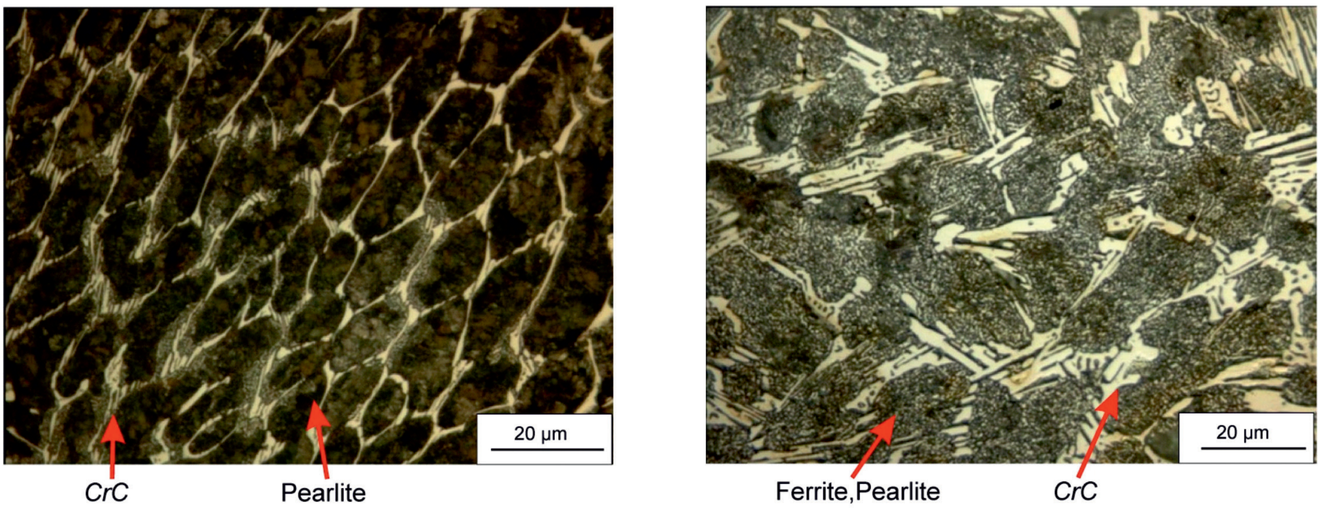

a *b*

Fig. 8. Microstructure of *UTP A DUR 600* layers obtained after conventional *TIG* cladding (*a*) and *HFEMF*-assisted *TIG* cladding (*b*). Etched with 3% picral; magnification ×1,000; scale bar: 20 µm

The deposited *UTP A DUR 600* layer is characterized by the presence of chromium-containing hard phases formed during rapid solidification. Due to the high chromium content of the filler wire, carbide-forming reactions occur within the molten pool, resulting in the formation of chromium-rich carbide constituents embedded in an iron-based matrix.

The conventionally deposited layer exhibits a relatively heterogeneous distribution of carbide-containing regions, which is related to insufficient mixing of chromium and carbon during solidification. In contrast, *HFEMF*-assisted processing is considered to promote enhanced melt-pool convection, resulting in improved redistribution of chromium-rich constituents and more uniform carbide morphology.

The increased hardness observed after *HFEMF*-assisted *UTP A DUR 600* cladding is therefore attributed not to the generation of a completely new phase structure, but to a more favorable distribution and formation of chromium-rich carbide phases during solidification.

Figs. 9, *a* and *b* present the microstructures of *Ni78Si8B14*-alloyed *EN-GJV-400* surfaces obtained without and with *HFEMF* assistance.

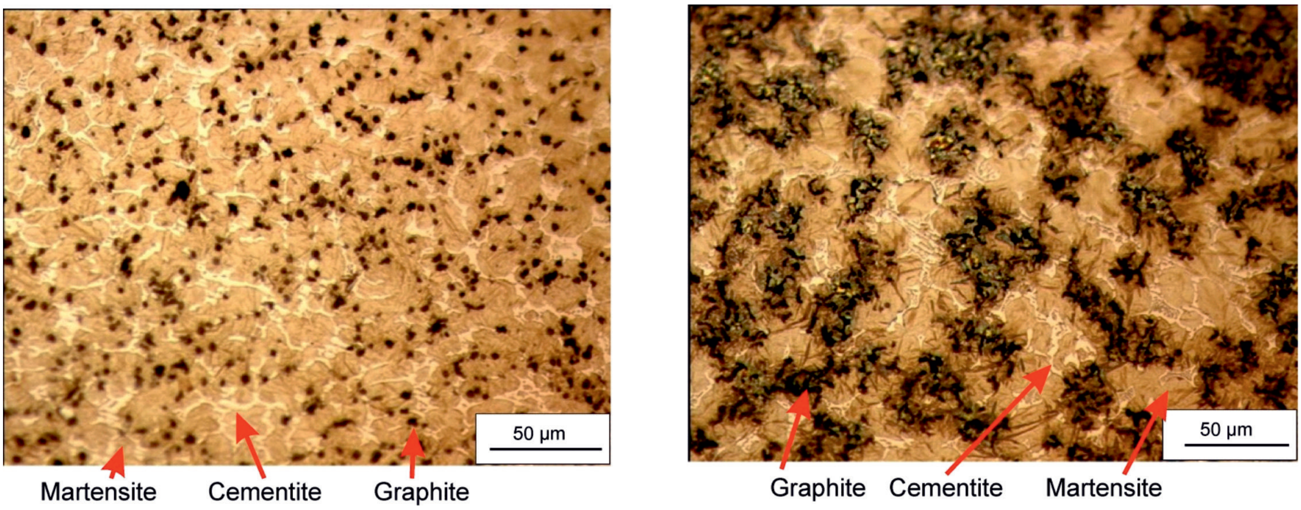

a *b*

Fig. 9. Microstructure of *Ni78Si8B14*-alloyed *EN-GJV-400* surface layers obtained after conventional *TIG* treatment (*a*) and *HFEMF*-assisted *TIG* treatment (*b*). Etched with 4% nital; magnification ×500; scale bar: 50 μm

The introduction of *Ni*, *Si*, and *B* modifies the chemical composition of the molten zone and increases its hardenability. During rapid cooling, the alloyed layer may contain martensitic transformation products together with ledeburitic eutectic constituents and carbide-containing regions.

The conventionally alloyed layer demonstrates local variations in phase morphology caused by non-uniform distribution of alloying elements. *HFEMF*-assisted processing improves liquid-phase mixing and promotes a more homogeneous distribution of nickel-, silicon-, and boron-containing regions.

The role of *HFEMF* during *Ni* alloying is therefore related mainly to improved chemical homogenization and stabilization of the resulting microstructure rather than to direct formation of additional hard phases.

Fig. 10 presents the microstructures obtained after *CuSn-4* alloying with and without *HFEMF* assistance.

Copper addition influences the solidification behavior of the modified layer and contributes to the modification of the surface properties. Unlike chromium-containing cladding materials, copper alloying is not primarily intended to increase hardness. The main objective of *Cu* introduction is related to the modification of tribological behavior, including the formation of copper-containing transfer layers during sliding contact and preservation of beneficial graphite-related lubricating effects.

The conventionally alloyed layer exhibits local variations in copper-containing regions due to limited melt homogenization. *HFEMF*-assisted processing improves the redistribution of copper within the molten zone, resulting in a more uniform microstructural appearance.

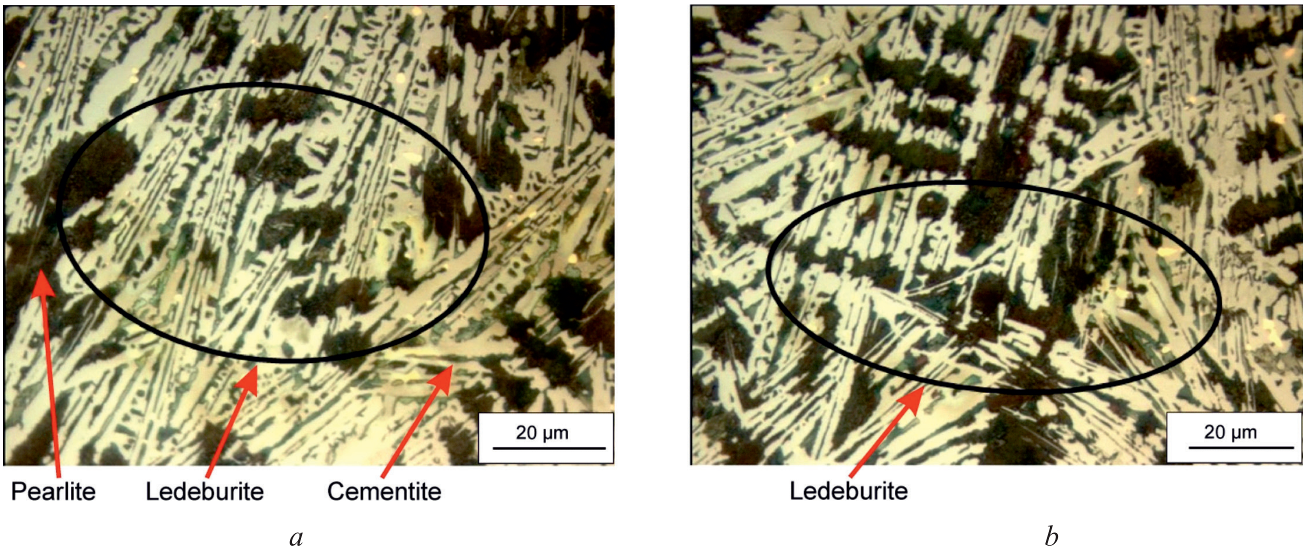

Fig. 10. Microstructure of *CuSn-4*-alloyed *EN-GJV-400* surface layers obtained after conventional *TIG* treatment (*a*) and *HFEMF*-assisted *TIG* treatment (*b*). Etched with 3% nital; magnification ×1,000; scale bar: 20 μm

Overall, the obtained results demonstrate that *HFEMF* acts primarily as a melt-pool control mechanism. The electromagnetic stirring modifies heat and mass transfer conditions, reduces local segregation, and improves structural uniformity. The final microstructural response depends strongly on the chemical composition of the modified layer: homogenization dominates during remelting and alloying, whereas carbide redistribution becomes the controlling factor during chromium-rich cladding.

Chemical composition and elemental redistribution (EDS analysis)

Energy-dispersive X-ray spectroscopy (*EDS*) analysis was performed to evaluate the incorporation and redistribution of alloying elements within the *TIG*-modified surface layers and to determine the influence of *HFEMF* assistance on chemical homogeneity during melting and subsequent solidification.

The obtained elemental concentrations were analysed in comparison with the initial chemical composition of the *EN-GJV-400* substrate presented in Table 1. The base material contains mainly *Fe*, *C*, *Si*, *Mn*, *Cu*, and *Ni*, with very low chromium content. After surface modification, additional variations in the concentration of *Ni*, *Cu*, and *Cr* were observed depending on the applied processing route.

The *EDS* results confirmed the presence of the characteristic elements of the *EN-GJV-400* matrix and demonstrated the successful incorporation of alloying elements introduced during surface treatment. The measured elemental distributions across different regions of the modified layers are summarized in Table 8. The comparison between the surface, middle region, and fusion zone indicates that *HFEMF*-assisted processing influences the spatial distribution of alloying elements by modifying melt-pool convection during melting and solidification.

For conventional *TIG* remelting of *EN-GJV-400*, no external alloying elements were introduced into the molten pool. Therefore, the observed structural changes are mainly associated with dissolution of graphite particles, redistribution of carbon, and rapid non-equilibrium solidification. The *EDS* analysis did not reveal significant variations in the overall chemical composition after *HFEMF* application; however, electromagnetic stirring contributed to a more uniform distribution of dissolved elements within the remelted zone. This behavior is consistent with the observed homogenization of the ledeburitic surface structure formed during rapid solidification.

In *Ni78Si8B14*-alloyed layers, *EDS* analysis demonstrated a significant increase in nickel concentration compared with the initial *EN-GJV-400* composition given in Table 1. The distribution of nickel within the modified layer was relatively uniform, indicating improved transport of alloying elements under *HFEMF*-assisted conditions. *EDS* analysis confirmed a relatively uniform redistribution of *Ni* and *Si* within the alloyed layer. Since boron cannot be reliably quantified by conventional *EDS* because of its low atomic

Table 8

Representative *EDS*-measured elemental distribution in selected *TIG*-modified *EN-GJV-400* surface layers

Material	Position in layer	*Sn* (%)	*Al* (%)	*Si* (%)	*Mn* (%)	*Ni* (%)	*Cu* (%)	*Cr* (%)	*Fe* (%)
EN-GJV-400 (base material)	–	–	0.09	2.41	0.49	0.26	0.67	0.09	Balance
Cu-based alloying (*CuSn-4*)	Fusion zone	0.06	0.07	2.15	0.45	0.29	7.15	0.05	Balance
	Central part of modified layer	0.05	0.04	2.17	0.43	0.41	8.57	0.06	Balance
	Surface	0.08	0.09	2.41	0.49	0.32	9.10	0.07	Balance
Ni-based alloying (*Ni78Si8B14*)	Fusion zone	–	0.07	2.56	0.40	8.23	0.61	0.07	Balance
	Central part of modified layer	–	0.08	2.43	0.44	9.11	0.72	0.06	Balance
	Surface	–	0.10	2.34	0.49	9.32	0.68	0.09	Balance

number, its presence was inferred from the nominal composition of the *Ni78Si8B14* alloy rather than from direct elemental measurements. Consequently, the contribution of boron to phase formation is discussed only qualitatively and in combination with the observed microstructural features and hardness evolution. The observed martensitic-type constituents and carbide-containing regions are consistent with the increased hardenability expected from the nominal *Ni–Si–B* alloy composition; however, the specific contribution of boron cannot be verified directly by the present *EDS* analysis.

For *CuSn-4* alloying, the *EDS* results showed effective incorporation and redistribution of copper within the modified layer. Unlike chromium- or nickel-containing alloy systems, the purpose of copper addition was not primarily to maximize hardness, but to modify the surface behavior while maintaining the beneficial role of graphite-containing regions. The preservation of graphite-containing regions may be beneficial for future tribological performance because graphite is widely recognized as a solid lubricant in cast irons. However, no tribological tests were carried out in the present study; therefore, any improvement in friction or wear behavior should be regarded as a hypothesis inferred from the observed microstructure rather than as an experimentally verified result. *HFEMF*-assisted processing contributed to a more uniform distribution of copper-containing regions by enhancing melt-pool mixing.

The *EDS* analysis of *UTP A DUR 600* cladded layers revealed a significant increase in chromium content compared with the initial *EN-GJV-400* substrate (Table 1). Chromium is the main carbide-forming element responsible for the development of wear-resistant hard phases in the deposited layer. Under conventional *TIG* cladding conditions, variations in chromium distribution may occur due to limited melt-pool circulation and local differences in solidification conditions. The application of *HFEMF* improved the redistribution of chromium within the molten pool, resulting in a more homogeneous distribution of chromium-rich regions.

The improved chromium distribution under electromagnetic stirring provides more favorable conditions for the formation and spatial uniformity of chromium-containing carbide phases observed in the microstructural analysis. This effect explains the increase in average hardness from 771 *HV0.1* for conventional *UTP A DUR 600* cladding to 800 *HV0.1* for *HFEMF*-assisted cladding.

Overall, the *EDS* results demonstrate that *HFEMF* does not modify the chemical composition of the material by introducing new elements. Instead, it acts as a process-control parameter that changes the transport conditions inside the molten pool, enhances alloying-element redistribution, reduces local chemical heterogeneity, and promotes a more uniform development of strengthening phases when carbide-forming elements are present.

Microhardness distribution and structural homogenization

Microhardness measurements were performed to evaluate the mechanical response of the modified surface layers and to clarify the influence of *HFEMF* assistance on hardness evolution and structural uniformity. The measurements were carried out using a *PMT-3 Vickers* microhardness tester under a load of 0.98 N (*HV0.1*) with a dwell time of 15 s. For each processing condition, ten indentations were performed at different positions across the modified layer, including the surface region, the central part of the remelted or deposited zone, and the transition region between the modified layer and the *EN-GJV-400* substrate. The reported values represent the average hardness obtained from these measurements, while the standard deviation was calculated from the individual measurements for each condition.

The average microhardness values of the investigated surface modification conditions, including the corresponding standard deviation values, are presented in Fig. 11. The cross-sectional variation of microhardness across representative surface-modified layers is shown in Fig. 12 to evaluate the spatial distribution of hardness and the influence of *HFEMF* on structural uniformity.

The untreated *EN-GJV-400* substrate exhibited an average hardness of approximately 375 *HV0.1*, corresponding to its initial ferritic-pearlitic matrix containing vermicular graphite. After *TIG*-based surface modification, all investigated conditions demonstrated a significant increase in hardness due to rapid melting, partial dissolution of graphite, carbon redistribution, and non-equilibrium solidification of the modified surface region.

As shown in Fig. 11, conventional *TIG* remelting increased the average hardness of *EN-GJV-400* from approximately 375 *HV0.1* to 765 *HV0.1*. This increase was mainly associated with the transformation of the initial ferritic-pearlitic structure into a hardened remelted layer containing ledeburitic eutectic constituents with cementite-rich phases. During rapid cooling, carbon released from partially dissolved graphite particles increases the carbon content of the molten region, promoting the formation of hard carbide-containing structures responsible for the increased hardness.

The application of *HFEMF* during *TIG* remelting resulted in a comparable hardness level of approximately 760 *HV0.1*. The absence of a significant difference between conventional and *HFEMF*-assisted remelting indicates that electromagnetic assistance does not provide an independent strengthening effect. Instead, the main contribution of *HFEMF* is associated with modification of molten-pool transport phenomena, improving heat and mass transfer conditions, and promoting a more uniform distribution of the solidification products.

The hardness distribution presented in Fig. 12 further supports this interpretation. Although both conventional and *HFEMF*-assisted remelting produced a hardened surface region, the *HFEMF*-assisted

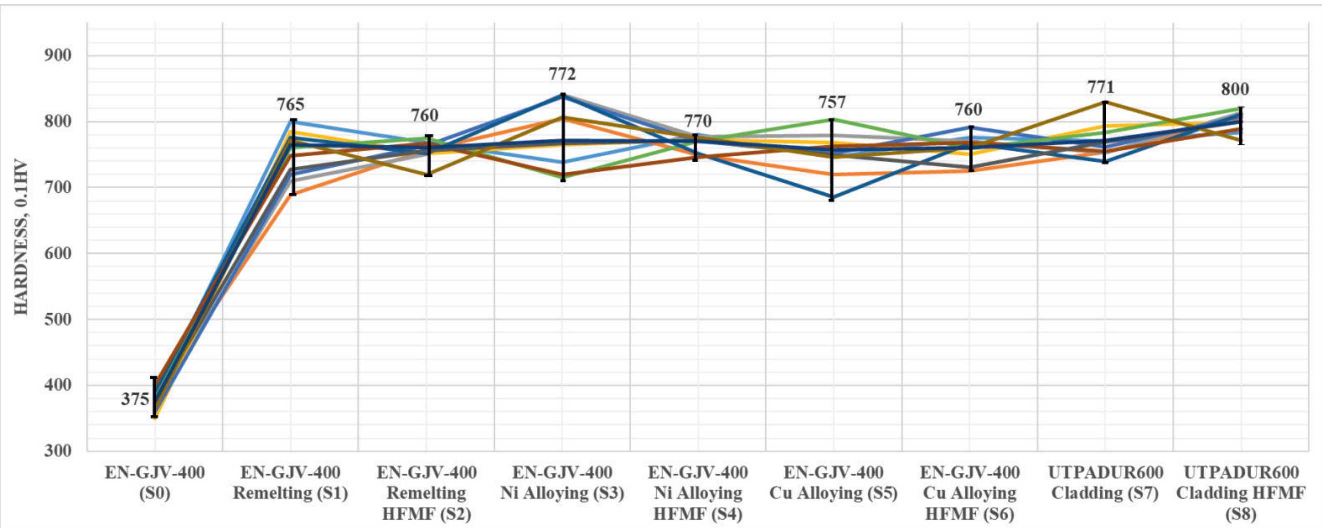

Fig. 11. Average *Vickers* microhardness values with standard deviation error bars for *EN-GJV-400* surface layers after conventional and *HFEMF*-assisted *TIG* surface modification treatments

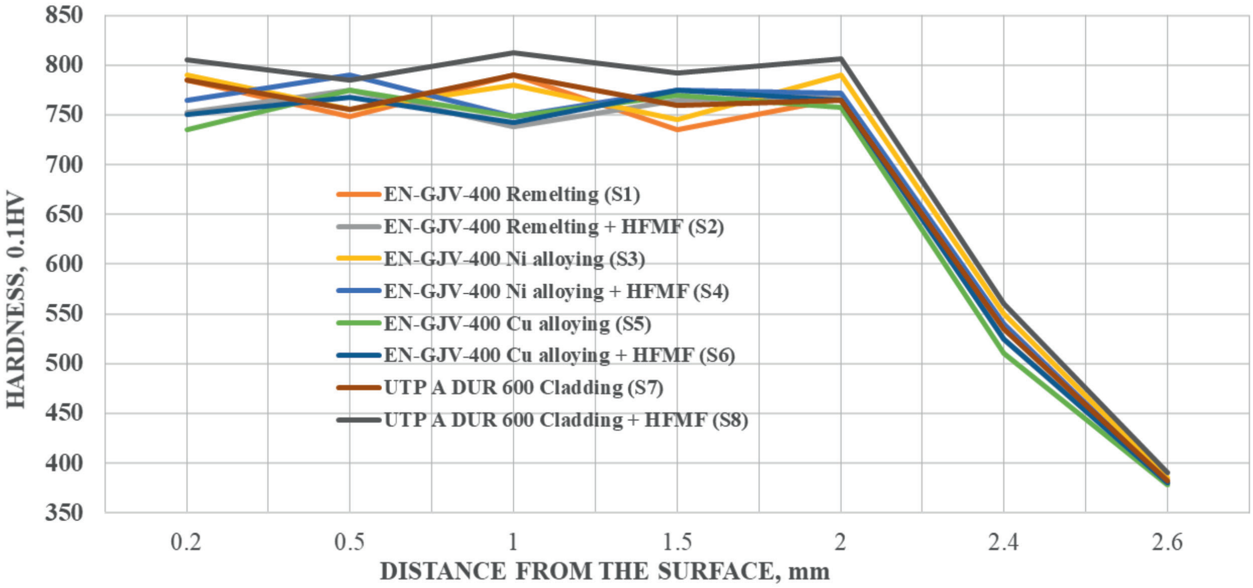

Fig. 12. Microhardness variation across the cross-section of surface-modified *EN-GJV-400* compacted graphite iron

layer exhibited a more uniform hardness profile across the modified zone. The reduced local variations in hardness can be attributed to improved melt homogenization and more uniform distribution of carbon-rich eutectic constituents during solidification. Therefore, the effect of *HFEMF* during remelting is mainly related to structural stabilization rather than hardness enhancement.

The *Ni78Si8B14*-alloyed layer exhibited an average hardness of approximately 772 *HV0.1*, while the corresponding *HFEMF*-assisted condition showed a slightly lower value of approximately 770 *HV0.1* (Fig. 11). The obtained hardness level is associated with the combined effect of nickel, silicon, and boron additions, which modify the chemical composition of the molten zone and promote the formation of martensitic-type transformation products together with ledeburitic eutectic and carbide-containing constituents during rapid cooling. The small difference between conventional and *HFEMF*-assisted conditions confirms that electromagnetic stirring mainly affects the spatial distribution and uniformity of these phases rather than their fundamental formation mechanism.

The cross-sectional hardness profiles of *Ni78Si8B14*-alloyed layers (Fig. 12) indicate that *HFEMF*-assisted processing reduces local hardness fluctuations within the modified zone. This behavior is consistent with the *SEM*/*EDS* observations, demonstrating improved redistribution of alloying elements and a more homogeneous development of strengthening constituents.

The *CuSn-4*-alloyed layer demonstrated hardness values of approximately 757 *HV0.1* without *HFEMF* and 760 *HV0.1* with *HFEMF* assistance. Compared with *Ni*- and *Cr*-containing systems, copper alloying does not significantly contribute to hardness enhancement because its main purpose is related to modification of surface functional behavior rather than formation of hard phases. The presence of *Cu*-rich regions together with retained graphite-containing areas may provide favorable conditions for future tribological performance; however, this assumption requires confirmation through dedicated friction and wear investigations.

The *UTP A DUR 600* cladded layers demonstrated a different response to *HFEMF* assistance. According to Fig. 11, the conventional *TIG* cladding condition exhibited an average hardness of approximately 771 *HV0.1*, whereas *HFEMF*-assisted cladding increased the hardness to approximately 800 *HV0.1*. This increase is attributed to improved redistribution and more uniform formation of chromium-containing hard phases during solidification. Although the filler wire contains approximately 9.5 wt.% *Cr*, electromagnetic-assisted melt stirring promotes more homogeneous transport of chromium within the molten pool, providing favorable conditions for carbide-containing constituent formation.

The hardness profiles shown in Fig. 12 confirm that the *HFEMF*-assisted *UTP A DUR 600* layer possesses a more stable hardness distribution compared with the conventionally deposited layer. The reduced variation of hardness values across the deposited region indicates a more homogeneous distribution of chromium-rich strengthening phases, which is consistent with the *SEM*/*EDS* results.

The comparison of all investigated conditions demonstrates that the influence of *HFEMF* on hardness is strongly dependent on the chemical composition of the modified layer and the dominant strengthening mechanism. For direct TIG remelting and *Ni*/*Cu* alloying, electromagnetic assistance primarily improves structural homogenization and reduces local hardness variations without significantly changing the average hardness value. In contrast, for chromium-rich *UTP A DUR 600* cladding, *HFEMF* contributes simultaneously to structural homogenization and hardness enhancement through improved carbide-phase distribution.

Therefore, the principal role of *HFEMF* assistance is not a universal increase in hardness, but rather a controlled modification of melt-pool dynamics, elemental redistribution, and phase homogeneity. The combination of average hardness values (Fig. 11) and cross-sectional hardness profiles (Fig. 12) confirms that *HFEMF* provides an additional process-control parameter capable of stabilizing the structure–property relationship of *TIG*-modified *EN-GJV-400* surfaces.

Role of HFEMF in structure formation during TIG surface modification and practical implications

During conventional *TIG* surface modification of *EN-GJV-400* compacted graphite iron, the formation of the modified surface layer is governed by the interaction of arc heat input, melting and solidification kinetics, surface-tension-driven convection, buoyancy forces, and gravitational effects. These phenomena determine the geometry of the molten region, thermal gradients, solute redistribution, and the morphology of the final solidification products. However, in conventional *TIG* processing, liquid-phase transport is controlled mainly by natural convection mechanisms, which may result in local differences in chemical composition and heterogeneous distribution of structural constituents, particularly when processing components with complex geometries such as camshaft surfaces.

The application of an *HFEMF* introduces an additional physical interaction between the externally generated magnetic field and the electrically conductive molten region. According to magnetohydrodynamic principles, electrical currents induced within the molten metal interact with the applied magnetic field, generating electromagnetic forces that may influence liquid-phase transport phenomena. These interactions can modify the conditions of melt-pool mixing, solute redistribution, and solidification. However, in the present study, the transient melt-pool velocity field, local electromagnetic force distribution, and dynamic flow behavior were not directly measured. Therefore, the influence of *HFEMF* was evaluated indirectly based on experimentally obtained surface morphology, microstructural characteristics, elemental distribution, and microhardness response.

The obtained results demonstrate that *HFEMF* does not fundamentally alter the phase formation mechanisms occurring during *TIG* processing of *EN-GJV-400* compacted graphite iron. Instead, its main contribution is related to modification of the conditions under which melting, mixing, and solidification occur. The effectiveness of electromagnetic assistance depends strongly on the chemical composition of the modified layer and the dominant strengthening mechanism associated with each processing route.

During conventional *TIG* remelting of *EN-GJV-400*, the initial ferritic-pearlitic matrix containing vermicular graphite was transformed into a hardened surface layer consisting mainly of ledeburitic eutectic constituents with cementite-rich phases. This transformation occurred due to partial graphite dissolution, carbon redistribution within the molten region, and rapid non-equilibrium solidification. The average hardness increased from approximately 375 *HV0.1* for the untreated substrate to approximately 765 *HV0.1* after conventional *TIG* remelting. The application of *HFEMF* resulted in a similar hardness value of approximately 760 *HV0.1*. The absence of a significant hardness difference indicates that electromagnetic assistance does not act as an independent strengthening mechanism. Instead, the observed microstructural differences suggest that *HFEMF* contributes mainly to improved uniformity of the solidification products within the modified layer.

A similar tendency was observed for *Ni78Si8B14* surface alloying. The introduction of *Ni*, *Si*, and *B* modified the chemical composition of the molten region and increased its hardenability, favoring the formation of hardened transformation products together with ledeburitic and carbide-containing constituents during rapid cooling. The close hardness values obtained for conventional alloying and *HFEMF*-assisted alloying (approximately 772 and 770 *HV0.1*, respectively) indicate that *HFEMF* does not significantly change the overall strengthening mechanism. Its primary role is associated with improved redistribution and homogenization of alloying elements within the molten region. Since boron cannot be reliably quantified by conventional *EDS* analysis, its contribution to phase formation is interpreted qualitatively based on the nominal *Ni78Si8B14* composition, microstructural observations, and hardness measurements.

For *CuSn-4* alloying, the influence of *HFEMF* was mainly associated with the distribution of copper-containing regions within the modified layer. Unlike chromium-containing cladding systems, copper alloying was not introduced primarily to maximize hardness but to modify the functional characteristics of the surface. The obtained results indicate that *HFEMF* contributes to a more uniform distribution of copper within the alloyed region. However, the expected influence of *Cu*-rich regions and retained graphite on tribological behavior remains a hypothesis requiring confirmation through dedicated friction and wear investigations.

A different response was observed for *UTP A DUR 600* cladding. In this case, the chemical composition of the deposited layer provides a stronger contribution to hardness development due to the presence of chromium as a carbide-forming element. The conventional cladded layer exhibited an average hardness of approximately 771 *HV0.1*, whereas *HFEMF*-assisted processing increased the hardness to approximately 800 *HV0.1*. This improvement is associated with a more homogeneous distribution of chromium-containing hard phases within the deposited layer. The results indicate that *HFEMF* does not introduce a new strengthening mechanism but modifies the conditions of alloy-element redistribution and solidification, favoring a more uniform formation of carbide-containing constituents.

The comparison of all investigated surface modification routes demonstrates that the influence of *HFEMF* depends on the interaction between electromagnetic assistance and the chemical characteristics of the modified layer. When the strengthening mechanism is mainly controlled by rapid solidification of the substrate material, as in *TIG* remelting, *HFEMF* primarily contributes to structural homogenization. When alloying elements with strong phase-forming capability are introduced, electromagnetic assistance affects their spatial redistribution and the uniformity of the resulting phases. The main differences between the investigated processing conditions are summarized in Table 9.

The comparison presented in Table 9 confirms that *HFEMF*-assisted *TIG* processing should primarily be considered as a process-control approach rather than a direct hardness-enhancement method. Its main contribution is associated with modifying transport conditions during melting and solidification, which can improve the uniformity of elemental distribution and phase morphology. The influence on mechanical properties depends on the dominant strengthening mechanism of the modified layer.

From the viewpoint of surface engineering, the main advantage of *HFEMF*-assisted *TIG* processing is the possibility of influencing surface-layer development without changing the bulk composition of the component. The improved structural uniformity observed after electromagnetic assistance may contribute to more stable and reproducible surface properties. For automotive and heavy-duty applications involving compacted graphite iron components, including camshaft surfaces, *HFEMF*-assisted *TIG* processing provides an additional parameter for controlling the formation of functional surface layers.

Nevertheless, further investigations involving direct observation of molten-pool behavior, numerical modelling of electromagnetic interactions, and systematic tribological testing are required to establish quantitative relationships between electromagnetic parameters, melt-pool transport phenomena, and final functional properties of modified surfaces.

Table 9

Comparison of conventional and *HFEMF*-assisted *TIG* surface modification of *EN-GJV-400* compacted graphite iron

Treatment condition	Key governing factors	Observed effect of *HFEMF*	Obtained material response
Conventional *TIG* remelting	Thermal cycle, graphite dissolution, carbon redistribution, and natural melt transfer	Reference state without external control of liquid-phase transfer	Formation of a hardened ledeburite layer with cementite-containing phases; hardness ≈765 *HV0.1*
TIG remelting + *HFEMF*	Thermal effect combined with electromagnetic interaction in the electrically conductive molten zone	Improvement of structural constituent uniformity and reduction of local solidification differences	Comparable hardness level (≈760 *HV0.1*), indicating primarily structural homogenization
Ni78Si8B14 + *HFEMF*	Phase formation under alloying combined with electromagnetic redistribution of elements	More uniform distribution of *Ni–Si*-containing regions and transformation products	Comparable hardness (≈770 *HV0.1*); enhanced structural uniformity
CuSn-4 + *HFEMF*	Copper introduction, solidification characteristics, and influence of graphite-containing regions	More uniform distribution of *Cu*-containing regions	Comparable hardness (≈760 *HV0.1*); possible influence on tribology requires further verification
UTP A DUR 600 + *HFEMF*	Formation of chromium-containing phases and carbide strengthening	Improved spatial distribution of chromium-containing hard phases	Hardness increase (≈771 → 800 *HV0.1*) due to more uniform distribution of strengthening phases

Conclusions

Based on the experimental investigation of conventional and *HFEMF*-assisted *TIG* surface modification of *EN-GJV-400* compacted graphite iron, the following conclusions can be drawn:

1. The application of a 200 kHz *HFEMF* during *TIG* surface modification provides an additional process-control parameter for influencing surface-layer formation and structural development in *EN-GJV-400* compacted graphite iron. The effect of *HFEMF* was identified through changes in surface morphology, microstructural uniformity, elemental distribution, and hardness response. Since direct measurements of molten-pool velocity and electromagnetic forces were not performed, the influence of *HFEMF* was evaluated indirectly through the resulting characteristics of the solidified layers.

2. *TIG* remelting significantly modified the original ferritic-pearlitic structure of *EN-GJV-400* containing vermicular graphite. Graphite dissolution, carbon redistribution, and rapid non-equilibrium solidification resulted in the formation of hardened ledeburitic structures containing cementite-rich constituents. *HFEMF*-assisted remelting did not change the fundamental phase-formation mechanism but contributed to a more uniform distribution of solidification products within the modified layer.

3. The influence of *HFEMF* on alloyed and cladded layers was dependent on the chemical composition of the modified region and the dominant strengthening mechanism. *Ni78Si8B14* alloying promoted the formation of hardened transformation products together with ledeburitic and carbide-containing constituents, while *HFEMF* mainly improved the spatial distribution of alloying elements. *CuSn-4* alloying resulted in the formation of Cu-containing regions, for which possible improvements in tribological behavior require confirmation by dedicated wear investigations. For *UTP A DUR 600* cladding, *HFEMF* promoted a more uniform distribution of chromium-containing hard phases.

4. *SEM*/*EDS* analysis demonstrated that *HFEMF* does not introduce additional alloying elements into the modified layers. Instead, electromagnetic assistance affects the redistribution of introduced elements

during melting and solidification. Improved uniformity of *Ni*-, *Cu*-, and *Cr*-containing regions indicates reduced local chemical heterogeneity and more stable development of surface structures.

5. Microhardness measurements showed that all *TIG*-based surface modification treatments substantially increased the hardness of *EN-GJV-400* compacted graphite iron. The untreated substrate exhibited an average hardness of approximately 375 *HV0.1*, whereas the modified layers reached values between 757 and 800 *HV0.1*. Conventional *TIG* remelting produced approximately 765 *HV0.1*, while *HFEMF*-assisted remelting resulted in a comparable value of approximately 760 *HV0.1*, confirming that electromagnetic assistance primarily affects structural uniformity rather than hardness increase. The highest hardness value of approximately 800 *HV0.1* was achieved for *HFEMF*-assisted *UTP A DUR 600* cladding due to improved redistribution and more uniform formation of chromium-rich carbide-containing hard phases.

6. The established process–structure–property relationship confirms that *HFEMF*-assisted *TIG* processing can be used as a supplementary surface engineering approach for controlling microstructural homogeneity and phase distribution in *EN-GJV-400* compacted graphite iron. The beneficial effect of *HFEMF* is most pronounced in alloy systems where electromagnetic-assisted redistribution influences the formation and arrangement of strengthening phases, whereas in direct remelting processes its main contribution is structural homogenization.

References

1. König M. Literature review of microstructure formation in compacted graphite iron. *International Journal of Cast Metals Research*, 2010, vol. 23 (3), pp. 185–192. DOI: 10.1179/136404609X12535244328378.

2. Patel M., Dave K. An insight of compacted graphite iron (*CGI) characteristics and its production: A review. Recent* Advances in Manufacturing Processes and Systems. Singapore, Springer, 2022, pp. 131–148. ISBN 978-981-16-7787-8. DOI: 10.1007/978-981-16-7787-8_10.

3. Dawson S., Guesser W.L. Castability, product design and production of compacted graphite irons. *ASM Handbook*. Vol. 1A: *Cast Iron Science and Technology*. Materials Park, Ohio, ASM International, 2017. ISBN 978-1-62708-168-3. DOI: 10.31399/asm.hb.v01a.a0006328.

4. Bukhari S.M.A., Husnain N., Siddiqui F.A., Anwar M.T., Khosa A.A., Imran M., Qureshi T.H., Ahmad R. Effect of laser surface remelting on microstructure, mechanical properties and tribological properties of metals and alloys: A review. *Optics and Laser Technology*, 2023, vol. 165, p. 109588. DOI: 10.1016/j.optlastec.2023.109588.

5. Wollmann D., Pintaude G. Tribological performance of high-strength cast iron in lubricated contact containing carbon black. *Wear*, 2021, vol. 496–497, p. 203743. DOI: 10.1016/j.wear.2021.203743.

6. Gregorutti R.W., Grau J.E. Mechanical properties of compacted graphite cast iron with different microstructures. *International Journal of Cast Metals Research*, 2014, vol. 27 (5), pp. 275–281. DOI: 10.1179/1743133614Y.0000000118.

7. Chen Y., Pang J.C., Li S.X., Zou C.L., Zhang Z.F. Damage mechanism and fatigue strength prediction of compacted graphite iron with different microstructures. *International Journal of Fatigue*, 2022, vol. 164, p. 107126. DOI: 10.1016/j.ijfatigue.2022.107126.

8. Ray J., Acharyya S.K., Misra D. Surface modification of engineering materials using TIG cladding technique: A review. *Recent Advances in Manufacturing Engineering*. Singapore, Springer, 2025, pp. 173–183. ISBN 978-981-96-9767-0. DOI: 10.1007/978-981-96-9768-7_14.

9. Mitelea I., Bordeaşu I., Riemschneider E., Uţu I.D., Crăciunescu C.M. Cavitation erosion improvement following TIG surface-remelting of gray cast iron. *Wear*, 2022, vol. 496–497, p. 204282. DOI: 10.1016/j.wear.2022.204282.

10. Sun B., Cheng J., Cai Z., Zhao H., Zhang Z., Qu H., Zhang Q., Hong S., Liang X. Formation and wear property of broad-beam laser clad Fe-based coatings. *Surface and Coatings Technology*, 2021, vol. 405, p. 126598. DOI: 10.1016/j.surfcoat.2020.126598.

11. Rakhmonov J.U., Weiss D., Dunand D.C. Comparing evolution of precipitates and strength upon aging of cast and laser-remelted Al–8Ce–0.2Sc–0.1Zr alloys. *Materials Science and Engineering: A*, 2022, vol. 840, p. 142990. DOI: 10.1016/j.msea.2022.142990.

12. Song Y., Wu W., Yu Y., Hua L. Effects of electric and magnetic treatments on microstructures of solid metals: A review. *Chinese Journal of Mechanical Engineering*, 2023, vol. 36, p. 139. DOI: 10.1186/s10033-023-00961-y.

13. Lim Y.C., Yu X., Cho J.H., Sosa J., Farson D.F., Babu S.S., McCracken S., Flesner B. Effect of magnetic stirring on grain structure refinement. Part 1: Autogenous nickel alloy welds. *Science and Technology of Welding and Joining*, 2010, vol. 15 (7), pp. 583–589. DOI: 10.1179/136217110X12720264008277.

14. Tan C., Chen B., Liu F., Zhang X., Chen S., Song X. Numerical study on weld pool behaviors and keyhole dynamics in magnetic-field-assisted laser-arc hybrid welding of aluminum alloy. *Journal of Materials Research and Technology*, 2023, vol. 26, pp. 6446–6461. DOI: 10.1016/j.jmrt.2023.09.030.

15. Xu W., Shi Y., Cui Y., Liang Z. Effects of magnetic fields in arc welding, laser welding and resistance spot welding: A review. *Advanced Engineering Materials*, 2022, p. 2200682. DOI: 10.1002/adem.202200682.

16. Bai Q., Zhang K., Tian Y., Zhang J., Liu T., Liu Y., Wang B. Effect of Lorentz force distribution on solidified microstructure and segregation of magnesium alloys under pulsed electromagnetic field. *Journal of Alloys and Compounds*, 2025, vol. 1039, p. 183014. DOI: 10.1016/j.jallcom.2025.183014.

17. Meng X., Bachmann M., Artinov A., Rethmeier M. Experimental and numerical assessment of weld pool behavior and final microstructure in wire feed laser beam welding with electromagnetic stirring. *Journal of Manufacturing Processes*, 2019, vol. 45, pp. 408–418. DOI: 10.1016/j.jmapro.2019.07.021.

18. Zhang Z., Xu X., Ge P., Li K. Numerical modeling of electromagnetic field influences on fluid thermodynamic behavior and grain growth during solidification of 316L stainless steel laser-welded plates. *Metals*, 2025, vol. 15 (6), p. 609. DOI: 10.3390/met15060609.

19. Meng X., Bachmann M., Artinov A., Rethmeier M. The influence of magnetic field orientation on metal mixing in electromagnetic stirring enhanced wire feed laser beam welding. *Journal of Materials Processing Technology*, 2021, vol. 294, p. 117135. DOI: 10.1016/j.jmatprotec.2021.117135.

20. Balasubramani N., Venezuela J., StJohn D., Wang G., Dargusch M.A. A review of the origin of equiaxed grains during solidification under mechanical stirring, vibration, electromagnetic, electric-current and ultrasonic treatments. *Journal of Materials Science & Technology*, 2023, vol. 144, pp. 243–265. DOI: 10.1016/j.jmst.2022.09.067.

21. Zhang H., Wu M., Rodrigues C.M.G., Ludwig A., Kharicha A., Rónaföldi A., Roósz A., Veres Z., Svéda M. Dendrite fragmentation mechanism under forced convection condition by rotating magnetic field during unidirectional solidification of AlSi7 alloy. *Acta Materialia*, 2022, vol. 241, p. 118391. DOI: 10.1016/j.actamat.2022.118391.

22. Adelian A., Ranjbar K., Reihanian M., Dehmolaei R. Microstructural refinement and mechanical enhancement of Hastelloy X welds via electromagnetic vibration-assisted GTAW. *Journal of Materials Research and Technology*, 2025, vol. 37, pp. 2750–2763. DOI: 10.1016/j.jmrt.2025.06.213.

Conflicts of Interest

The author declares no conflict of interest.